

Ferromagnetically Coupled Shastry-Sutherland Quantum Spin Singlets in (CuCl)LaNb₂O₇

C. Tassel,¹ J. Kang,² C. Lee,² O. Hernandez,³ Y. Qiu,⁴ W. Paulus,³ E. Collet,⁵ B. Lake,^{6,7} T. Guidi,^{6,8}
M.-H. Whangbo,² C. Ritter,⁹ H. Kageyama,¹ and S.-H. Lee¹⁰

¹Department of Energy and Hydrocarbon Chemistry, Graduate School of Engineering, Kyoto University, Kyoto 615-8510, Japan

²Department of Chemistry, North Carolina State University, Raleigh, North Carolina 27695-8204, USA

³University of Rennes 1, Sciences Chimiques de Rennes UMR CNRS 6226, Campus de Beaulieu, 35042 Rennes, France

⁴NIST Center for Neutron Research, National Institute of Standards and Technology, Gaithersburg, Maryland 20899, USA

⁵University of Rennes 1, Institut de Physique de Rennes UMR CNRS 6251, Campus de Beaulieu, 35042 Rennes, France

⁶Helmholtz-Zentrum Berlin für Materialien und Energie, Hahn Meitner Platz 1, Berlin 14109, Germany

⁷Institut für Festkörperphysik, Technische Universität Berlin, Hardenbergstrabe 36, 10623 Berlin, Germany

⁸ISIS Facility, Rutherford Appleton Laboratory, Chilton, Didcot, Oxon OX11 0QX, United Kingdom

⁹Institut Laue Langevin, BP 156, 38042 Grenoble, France

¹⁰Department of Physics, University of Virginia, Charlottesville, Virginia 22904-4714, USA

(Received 31 May 2010; revised manuscript received 29 July 2010; published 14 October 2010)

A thorough crystal structure determination at very low temperature of (CuCl)LaNb₂O₇, originally proposed as a spin-1/2 square-lattice antiferromagnet, is reported thanks to the use of single-crystal x-ray diffraction and powder neutron diffraction. State-of-the-art calculations (maximum entropy method) reveal that (CuCl)LaNb₂O₇ is orthorhombic with *Pbam* symmetry. First-principles calculations demonstrate that the dominant magnetic interactions are antiferromagnetic between fourth nearest neighbors with a Cu-Cl-Cl-Cu exchange path, which lead to the formation of spin singlets. The two strongest interactions between the singlets are ferromagnetic, which makes (CuCl)LaNb₂O₇ the first system of ferromagnetically coupled Shastry-Sutherland quantum spin singlets.

DOI: 10.1103/PhysRevLett.105.167205

PACS numbers: 75.10.Jm, 75.10.Kt

Frustrated quantum magnets continue to attract interest due to the wide range of exotic ground states and excitations that they display [1]. Here the magnetic ions have low spin values (typically spin-1/2 or 1) and are coupled together by competing interactions. For example, the kagome and pyrochlore lattices combined with antiferromagnetic couplings give rise to novel behavior because it is impossible to simultaneously satisfy all interactions [2]. Frustration is also possible in dimerized systems where the dominant coupling pairs the spins into singlets and the interdimer couplings are antiferromagnetic and competing. An example is the Shastry-Sutherland system; here the dimerization gives rise to gapped triplon excitations and the frustration suppresses triplon hopping [3]. A rich series of ground states are found in a magnetic field which map onto the fractal structure of the Hofstadter Butterfly [4]. Frustration is also possible in systems that have both ferromagnetic (FM) and antiferromagnetic (AFM) interactions, and can also result in novel phenomena; for example, a nematic order by two-magnon bound states has been predicted in a square lattice with competing FM and AFM interactions [5]. Experimental investigation of this type of systems is, however, lacking.

In 2005, (CuCl)LaNb₂O₇ was proposed as an example of spin-1/2 frustrated square lattice [6], along with other candidate materials [7,8]. Here the magnetic Cu²⁺ ions are octahedrally coordinated and form CuCl planes well separated by LaNb₂O₇ layers. The crystal symmetry was originally found to be tetragonal (space group *P4/mmm*) with

one copper ion per unit cell ($a_t = b_t = 3.88 \text{ \AA}$) forming an ideal undistorted square lattice [9]. Magnetic susceptibility, heat capacity, and neutron scattering revealed the absence of long range magnetic order and showed that the excitations are gapped and centered at 2.3 meV [6,10]. Further analysis indicated the presence of competing FM and AFM interactions, the former from the first-neighbor bond (J_1) and the latter from the second-neighbor bond (J_2). However, the experimental data appear to contradict the theory of the $J_1 - J_2$ model: gapped excitations are not expected except for a very limited region of the phase diagram when $J_1, J_2 > 0$, and $J_1/J_2 \approx 0.5$ [11], while a gapless spin disordered phase is predicted when $J_1 < 0, J_2 > 0$, and $J_1/J_2 \approx -0.5$ [5]. Recent NMR and transmission electron microscopy experiments suggested a possible orthorhombic distortion with doubling along both *a* and *b* axes which would allow for dimerization [12]. However, the proposed dimer pairing between first-neighbor copper ions is in contradiction with the observed fourth-neighbor dimerization [6].

This paper describes the first single-crystal growth of (CuCl)LaNb₂O₇ and a reinvestigation of the crystal structure by using x-ray and neutron diffraction which shows that the space group is in fact orthorhombic (*Pbam*) with considerable distortion of the Cu-Cl bonds and perovskite blocks. Band structure calculations reveal that the magnetism of this material is best described as antiferromagnetic dimers between fourth neighbors that are coupled together by frustrated ferromagnetic interactions in a Shastry-Sutherland-type arrangement.

A 15 g powder sample of $(\text{CuCl})\text{LaNb}_2\text{O}_7$ was synthesized by an ion-exchange reaction using a powder of $\text{RbLaNb}_2\text{O}_7$ and CuCl_2 , as described previously [9]. For single-crystal samples, precursor $\text{CsLaNb}_2\text{O}_7$ single crystals (Ref. [13]) with typical size of $0.5 \times 0.5 \times 0.1 \text{ mm}^3$ were embedded in a molar excess of CuCl_2 powder (99.99%) sealed in an evacuated tube and reacted at 340°C . Complete ion exchange to $(\text{CuCl})\text{LaNb}_2\text{O}_7$ was achieved after one week.

A CCD four-circle diffractometer was used for the x-ray single-crystal data collection at 14 K. Powder diffraction patterns were measured at 293 K and 2 K using neutrons of wavelength $\lambda = 1.9085 \text{ \AA}$ at D1A, ILL. Powder inelastic neutron scattering measurements were done with $\lambda = 3.8 \text{ \AA}$ on the disk-chopper-spectrometer at NCNR, NIST under an external magnetic field. The crystal structure was solved by direct methods using single crystal data and further refined by taking into account the twinning due to the pseudosymmetry. The structural parameters were optimized by a Rietveld refinement of neutron diffraction data (due to its higher sensitivity to O and Cl atoms). All the refinements were carried out using JANA2000 [14].

Figure 1(a) shows the inelastic neutron scattering data as a function of energy transfer, $\hbar\omega$. At $B = 0 \text{ T}$, a single gapped excitation centered at $\hbar\omega = 2.22(1) \text{ meV}$ is observed in agreement with previous work [6]. An external magnetic field of $B = 11.5 \text{ T}$ splits this peak into three peaks at $\hbar\omega = 1.19(1)$, $2.45(3)$, and $3.95(11) \text{ meV}$. The energies are consistent with the Zeeman splitting expected for a magnon excitation with spin $S = 1$ ($g\mu_B S_z B$). In zero field, the excitation extends in energy from $\sim 1.2 \text{ meV}$ to $\sim 3.0 \text{ meV}$ and is thus much broader than the resolution (0.16 meV), implying that it is dispersive due to interactions between dimers. Indeed the lower edge of the excitation is consistent with the critical field of $B_{c1} = 10.3 \text{ T}$

from magnetization measurements, for condensation of magnons into the ground state [10].

As shown in Fig. 1(b), the Q dependence exhibits a prominent peak centered at $Q_c \approx 0.5 \text{ \AA}^{-1}$. If we assume the dimers are noninteracting, the Q dependence goes as $1 - \frac{\sin Qr}{Qr}$ where r is the intradimer distance. The best fit to the data to the isolated spin dimer model was obtained with $r = 8.4(2) \text{ \AA}$ [black line in Fig. 1(b)] in agreement with previous work [6]. This reveals that the dominant magnetic interactions are between Cu^{2+} ions that are separated much further than the nearest neighbor (NN) distance of 3.88 \AA , a result that is inconsistent with the currently accepted structure of $(\text{CuCl})\text{LaNb}_2\text{O}_7$ [12].

To understand this unusual Q dependence, we have reinvestigated the crystal structure in great detail. Figure 2(a) shows the CCD image of the diffraction data taken for the $(hk0)$ plane at 14 K. Note that the crystal is twinned and thus h and k are interchangeable. Half-integer superlattice spots forbidden by $P4/mmm$ were found, indicating that the real unit cell is $2a_1 \times 2b_1 \times c$ compared to the tetragonal unit cell. Similar superreflections are also observed in the powder neutron diffraction pattern [Fig. 2(b)]. Superlattice peaks $(h, 0, 0)$ and $(0, k, 0)$ in the orthorhombic notation are absent when h and k are odd (red arrows). This extinction condition tells us that the crystal structure is orthorhombic with either $Pbam$ or $Pba2$ space group. The best fit to the x-ray and neutron diffraction data was obtained with the $Pbam$ structure, corroborated by less model-biased maximum entropy method maps. Table I lists the optimal structural parameters from the neutron diffraction data. Note that despite the lower crystal symmetry, there is still only one Cu^{2+} site in agreement with NMR [12]. The validity of the structural analysis is further supported by the bond valence sum calculation for copper yielding $+2.01$.

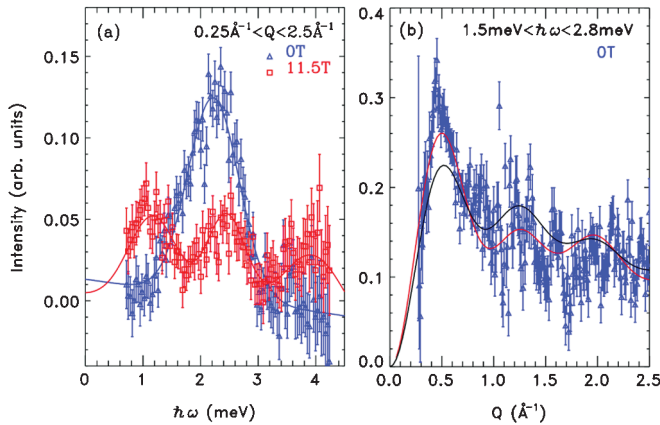


FIG. 1 (color). Inelastic neutron scattering data obtained at 70 mK from the powder sample. (a) Energy dependence of the triplet excitations for $B = 0 \text{ T}$ (blue) and $B = 11.5 \text{ T}$ (red). (b) Q dependence for $B = 0 \text{ T}$. Lines are described in the text.

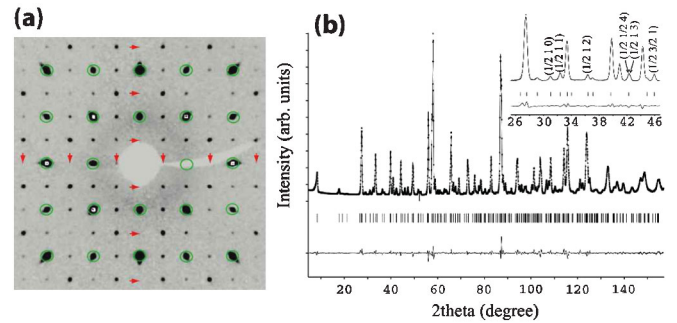


FIG. 2 (color). Single crystal x-ray and powder neutron diffraction data. (a) The x-ray CCD image of the ab plane at 14 K. The single crystal was twinned; thus a and b axes are interchangeable. The spots with green circles are the allowed integer Bragg reflections for the original tetragonal structure; the other spots are the half-integer reflections. (b) Rietveld plot against neutron diffraction data at 2 K. The indices in the inset are in the tetragonal notation.

TABLE I. Structural parameters obtained from Rietveld refinement of neutron diffraction at 2 K. *Pbam*, $a = 7.7556(5)$ Å, $b = 7.7507(5)$ Å, $c = 11.7142(4)$ Å, $R_{\text{Bragg}} = 1.64\%$, $R_{\text{wp}} = 4.62\%$, $R_p = 3.39\%$, and $\chi^2 = 3.38$.

Atom(<i>W</i>)	x/a	y/b	z/c	$U_{\text{iso}}(\text{Å}^2)$
Cu (4 <i>h</i>)	0.502(6)	0.7662(10)	0.5	0.0043(13)
Cl (4 <i>h</i>)	0.7367(16)	0.4286(7)	0.5	0.006(2)
La (4 <i>g</i>)	0.7412(11)	0.5001(10)	0	0.0024(12)
Nb (8 <i>i</i>)	0.500(3)	0.7529(9)	0.1908(3)	0.0040(9)
O1 (4 <i>f</i>)	0.5	0	0.1397(13)	0.002(3)
O2 (4 <i>e</i>)	0.5	0.5	0.1751(11)	0.008(3)
O3 (8 <i>i</i>)	0.752(4)	0.7509(11)	0.1545(10)	0.006(2)
O4 (4 <i>g</i>)	0.500(2)	0.7170(14)	0	0.007(2)
O5 (8 <i>i</i>)	0.501(4)	0.7731(11)	0.3410(5)	0.0089(16)

The refined orthorhombic crystal structure differs markedly from the tetragonal one previously reported. While the NbO_6 octahedra align with the axes in the tetragonal symmetry, they are strongly tilted in the orthorhombic structure, particularly around the a axis in a staggered manner [see Figs. 3(a) and 3(b)]. The tilting pattern of the NbO_6 strongly influences the positions of both the Cu and Cl atoms. In particular, the Cl atoms move significantly along the b direction and slightly along the a direction from their tetragonal position, probably to reduce Coulomb repulsion between chlorine and apical oxygen atoms. The Cu ions occupy the 4*h* sites. Along the a direction, they are mostly transversally displaced, i.e., along the b axis, yielding the distance between the NN Cu-Cu ions to be 3.626 Å and 4.129 Å along the b axis and 3.885 Å along the a axis. The Cu ion is coordinated octahedrally by two oxygen ligands with a distance of 1.865 Å as well as four chlorine ligands with two shorter bonds (2.386 Å, 2.389 Å) and two longer bonds (3.136 Å, 3.188 Å). When the local z and x axes for each Cu^{2+} ion are taken along the Cu-O and the short Cu-Cl bonds, respectively, the overall symmetry of the magnetic orbital including the ligand p orbitals has the $z^2 - x^2$ character. As a result, the spin exchange interactions in the CuCl layer become highly anisotropic.

We consider the Cu-Cl-Cu and Cu-Cl-Cl-Cu spin exchange paths in $(\text{CuCl})\text{LaNb}_2\text{O}_7$. In general, one expects that the Cu-Cl-Cu exchange is FM if the bond angle is close to 90° , and AFM if it deviates from 90° . However, when a Cu-Cl-Cu exchange path contains a long Cu-Cl bond (represented by Cl-Cu-Cl in Table II), the exchange becomes FM even if the Cl-Cu-Cl angle deviates considerably from 90° because the magnetic orbital is not contained in the long Cu-Cl bond [15,16]. The Cu-Cl-Cl-Cu spin exchange should become more strongly AFM with increasing Cu-Cl-Cl angle and shortening Cl-Cl contact distance so that the overlap between the Cl 3*p* orbitals in the Cl-Cl contact becomes large. The six exchanges considered in our study are listed in Table II and described in Fig. 3(c). To evaluate these exchanges, we determine the relative energies of seven possible ordered spin states of

TABLE II. Exchange paths for up to the fourth NN interactions in $(\text{CuCl})\text{LaNb}_2\text{O}_7$ and the corresponding coupling constants relative to J_4 . J_4 is AFM and of strength ~ 2.22 meV and a negative ratio of J_s/J_4 means that J_s is FM. Short and long lines between atoms represent different bond lengths without proportion.

J_s	path	d (Å)	angle ($^\circ$)	J_s/J_4
J_{1a}	Cu-Cl-Cu	3.885 48	108.9, 75.8	-0.39
J_{1b}	Cu-Cl-Cu	3.885 48	80.9	-0.04
J_{2a}	Cu-Cl-Cu	5.461 48	156.7	-0.38
J_{2b}	Cu-Cl-Cu	5.5053	170.2	-0.14
J_4	Cu-Cl-Cl-Cu	8.812 62	164.9	1
J'_4	Cu-Cl-Cl-Cu	8.532 50	150.0	0.18

$(\text{CuCl})\text{LaNb}_2\text{O}_7$ [see Fig. 3(d)] on the basis of density functional calculations employing the frozen-core projector augmented wave method [17,18] encoded in the VASP [19] with the generalized-gradient approximation (GGA) for the exchange-correlation functional [20]. The GGA plus on-site repulsion U (GGA + U) method [21] with effective $U = 4$ eV was used to properly describe the strong electron correlation of the Cu 3*d* states. By mapping the relative energies of the seven states determined from the GGA + U calculations onto the corresponding energies determined from the spin Hamiltonian defined in terms of the six exchanges, we obtain the values listed in Table II. The fourth NN interaction, J_4 , of the Cu-Cl-Cl-Cu exchange type is the strongest and is AFM. The other fourth NN coupling J'_4 is also AFM, but is much weaker than J_4 : $J'_4/J_4 = 0.18$. This is because J_4 has a larger Cu-Cl-Cl angle and a shorter Cl-Cl distance than J'_4 : 164.9° and 3.835 Å for J_4 vs 156.0° and 4.231 Å for J'_4 . All other J 's are FM. The strengths of the six exchanges decrease in the order, $J_4 > J_{1a} > J_{2a} > J'_4 > J_{2b} > J_{1b}$. Note that previous band structure calculations for $(\text{CuCl})\text{LaNb}_2\text{O}_7$ also found spatially anisotropic exchange interactions [22].

The fact that J_4 is both the strongest interaction and is AFM explains the long-standing mystery of the spin singlet formation in $(\text{CuCl})\text{LaNb}_2\text{O}_7$; the distance between the Cu ions connected by J_4 is indeed $r = 8.533$ Å, consistent with the intradimer distance obtained by the isolated dimer model [6]. To improve the model we considered the exchange paths J_{1a} and J_{2a} in addition to J_4 and fitted the inelastic neutron scattering data to the first moment sum rule for powder data [23]

$$\begin{aligned} \langle E(Q) \rangle &= \hbar^2 \int_{\Omega} \int_{\omega} \omega S(\mathbf{Q}, \omega) d\omega d\Omega \\ &\propto - \sum_s J_s \langle \mathbf{S}_0 \cdot \mathbf{S}_{d_s} \rangle |f_{\text{Cu}^{2+}}(Q)|^2 \left(1 - \frac{\sin Qd_s}{Qd_s} \right). \end{aligned}$$

In this equation the integration is over solid angle and energy, J_s is the exchange constant coupling the s th NN

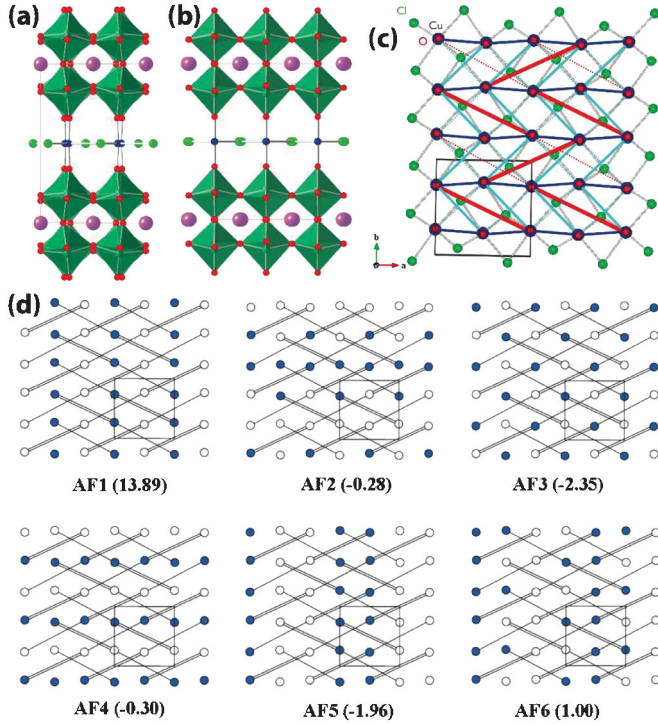


FIG. 3 (color). Crystal structure and magnetic exchange interactions of $(\text{CuCl})\text{LaNb}_2\text{O}_7$. (a) Projection of crystal structure in bc plane, (b) ac plane. Purple, red, blue, and green spheres represent La, O, Cu, and Cl ions, respectively. The dark green polygons represent NbO_6 octahedra. The grey lines show the unit cell. (c) Exchange interactions in the ab plane. The O ions are located above and below the Cu ions. The lines connecting Cu atoms represent exchange bonds: J_{1a} (blue), J_{2a} (solid cyan), J_{2b} (dotted cyan), J_4 (solid red), and J'_4 (dotted red). See Table II. J_{1b} is not plotted for clarity. (d) Six ordered AFM spin states used to extract the spin exchange parameters by GGA + U calculations. Only the Cu^{2+} ions are shown, and the open and filled circles represent the up and down spins, respectively. The relative energies (in meV per 4 f.u.) of the ordered spin states (with respect to the FM spin state) are given in the parentheses.

spins, d_s is their separation, and $\langle \mathbf{S}_0 \cdot \mathbf{S}_{d_s} \rangle$ is the two spin correlation function for this pair. Each coupling constant J_s produces a modulation in the first moment with a periodicity depending on the separation d_s of the spins, so that the dominant exchange interactions can be deduced although their absolute magnitudes cannot be determined. The best fit [red line, Fig. 1(b)] was obtained with $J_4 \langle \mathbf{S}_0 \cdot \mathbf{S}_{d_4} \rangle = 0.027(2)$, $J_{1a} \langle \mathbf{S}_0 \cdot \mathbf{S}_{d_{1a}} \rangle = 0.011(2)$, and $J_{2a} \langle \mathbf{S}_0 \cdot \mathbf{S}_{d_{2a}} \rangle = 0.005(2)$. Note that the ground state obtained by the first-principles calculations is the AF3 state shown in Fig. 3(d), and thus a positive value of $J_s \langle \mathbf{S}_0 \cdot \mathbf{S}_{d_s} \rangle$ indicates that the spin correlation agrees with the exchange constant; i.e., the spins are parallel for a FM interaction and antiparallel for an AFM interaction. The fit is much better than that of the simple dimer model, and the fitted parameters are consistent with our first-principles calculation results. This indicates that in $(\text{CuCl})\text{LaNb}_2\text{O}_7$, the fourth NN Cu^{2+}

ions form spin singlets, which are arranged orthogonally in the ab plane, while the coupling between them is primarily ferromagnetic.

Thus, the spin lattice of $(\text{CuCl})\text{LaNb}_2\text{O}_7$ is best described as ferromagnetically coupled Shastry-Sutherland quantum spin singlets. We anticipate our work will stimulate a theoretical investigation of the ferromagnetic Shastry-Sutherland system, as has been the case for the antiferromagnetic Shastry-Sutherland system exemplified by $\text{SrCu}_2(\text{BO}_3)_2$ [3]. Furthermore, related materials obtained by similar ion-exchange reactions have a wide variety of magnetic behaviors, including a fractional magnetization plateau in $(\text{CuBr})\text{Sr}_2\text{Nb}_3\text{O}_{10}$ and stripe order in $(\text{CuCl})\text{LaTa}_2\text{O}_7$. The present work provides a relevant starting model to capture the global features of magnetism in this ion-exchanged family.

Work at NCSU was supported by the DOE (DE-FG02-86ER45259) and by the resources of the NERSC and HPC Centers. Work at NCNR and UVA were supported by the U.S. NSF under Agreement No. DMR-0454672 and DMR-0903977, respectively. C. T. and H. K. acknowledge Science Research on Priority Area (19052004) from MEXT of Japan.

-
- [1] S. Sachdev, *Nature Phys.* **4**, 173 (2008), and references therein.
 - [2] R. Moessner, *Can. J. Phys.* **79**, 1283 (2001).
 - [3] S. Miyahara and K. Ueda, *J. Phys. Condens. Matter* **15**, R327 (2003).
 - [4] G. Misguich, T. Jolicoeur, S. M. Girvin, *Phys. Rev. Lett.* **87**, 097203 (2001).
 - [5] N. Shannon, T. Momoi, P. Sindzingre, *Phys. Rev. Lett.* **96**, 027213 (2006).
 - [6] H. Kageyama *et al.*, *J. Phys. Soc. Jpn.* **74**, 1702 (2005).
 - [7] N. Read and S. Sachdev, *Phys. Rev. Lett.* **62**, 1694 (1989).
 - [8] H. Rosner *et al.*, *Phys. Rev. Lett.* **88**, 186405 (2002).
 - [9] T. A. Kodendath *et al.*, *J. Am. Chem. Soc.* **121**, 10743 (1999).
 - [10] H. Kageyama *et al.*, *J. Phys. Soc. Jpn.* **74**, 3155 (2005).
 - [11] P. Sindzingre, *Phys. Rev. B* **69**, 094418 (2004).
 - [12] M. Yoshida *et al.*, *J. Phys. Soc. Jpn.* **76**, 104703 (2007).
 - [13] N. Kumada *et al.*, *Acta Crystallogr. Sect. C* **52**, 1063 (1996).
 - [14] <http://www-xray.fzu.cz/jana/jana.html>.
 - [15] M.-H. Whangbo and D. Dai, *Inorg. Chem.* **45**, 6227 (2006).
 - [16] M.-H. Whangbo *et al.*, *J. Solid State Chem.* **176**, 417 (2003).
 - [17] P. E. Blöchl, *Phys. Rev. B* **50**, 17953 (1994).
 - [18] G. Kresse and D. Joubert, *Phys. Rev. B* **59**, 1758 (1999).
 - [19] G. Kresse and J. Furthmüller, *Phys. Rev. B* **54**, 11169 (1996).
 - [20] J. P. Perdew, K. Burke, M. Ernzerhof, *Phys. Rev. Lett.* **77**, 3865 (1996).
 - [21] S. L. Dudarev *et al.*, *Phys. Rev. B* **57**, 1505 (1998).
 - [22] A. A. Tsirlin and H. Rosner, *Phys. Rev. B* **79**, 214416 (2009).
 - [23] P. Hohenberg and W. Brinkman, *Phys. Rev. B* **10**, 128 (1974).